Wafer-scale few layer graphene growth on Cu/Ni films for gas sensing applications

Geetanjali Deokar [1, 2*], Juan Casanova-Cháfer [3], Nitul S. Rajput [2], Cyril Aubry [2], Eduard Llobet [3], Mustapha Jouiad [2, 4*], Pedro M. F. J. Costa[1]

[1]Physical Science and Engineering Division, King Abdullah University of Science and Technology, Thuwal 23955-6900, Saudi Arabia

[2] Department of Materials & Engineering, Masdar Institute of Science and Technology-Khalifa University, Abu-Dhabi

[3] MINOS-EMaS, Universitat Rovira i Virgili, Tarragona, Spain

[4]LPMC-EA2081, University of Picardie Jules Vernes, Amiens, France

Abstract

Pristine, few-layer graphene (FLG)/Si nanopillar assemblies are introduced as gas sensitive chemiresistors showing unprecedented sensitivity towards NO_2 when operated at room temperature (25ºC) and in humid air. To achieve this, we first developed wafer-scale (~50 cm^2) FLG growth using sub-micrometer thick films of thermally evaporated Cu/Ni on a SiO_2/Si substrate. The Ni film was deposited and annealed to induce the formation of a Cu-rich binary alloy. This limited the inter-diffusion of Cu and SiO_2, a phenomenon known to take place during the CVD growth of graphene on Cu/SiO_2/Si. The as-grown high structural quality FLG was transferred, using a common wet chemical method, to lithographically patterned arrays of Si nanopillars (non-flat substrate). Testing of the FLG/Si assembly revealed a NO_2 sensitivity that outperforms what is reported in the literature for pristine graphene. Overall, our growth and device fabrication work-flow demonstrate a way to design graphene-based gas sensing systems without incurring inconvenient processing steps such as metal foil etching, surface functionalization or particle loading.

Keywords: Graphene, CuNi alloy, Chemical Vapor Deposition, Patterned Substrates, Gas Sensing

Corresponding authors: geetanjali.deokar@kaust.edu.sa;

mjouiad@masdar.ac.ae / mjouiad@gmail.com

1. Introduction

Graphene has a string of superlative qualities such as an extremely high charge carrier mobility, high thermal conductivity, extraordinary electrical and optical properties, etc. [1, 2]. In a case, for decades, graphene would become proponent in a wide range of applications such as electronics [1, 3], optoelectronics [4], supercapacitors [5], solar cells [6, 7], electrochemical sensing [8], and gas sensing [9-11]. Considering the latter, it has been repeatedly shown that graphene is uniquely suited because of its high surface area [doi:10.3390/app8071118] [DOI:10.1039/C2SC20205K]. However, the scale-up of the graphene-based sensors is constrained by synthesis limitation of the active material [doi:10.3390/app8071118]. It is currently consensual that to produce large area graphene with controlled structural quality, the chemical vapor deposition (CVD) technique is the most appropriate choice [REF. Roll to Roll]. In this respect, the most popular catalytic CVD substrate for single-layer graphene growth is the Cu metal foil. This is explained by the extremely low solubility of C in Cu at the temperature of the reaction, i.e. close to the melting point of Cu (1085ºC) [12, 13]. To progress beyond the lab-scale several bottlenecks remain in this approach. Furthermore, during the growth process, some of the Cu evaporates and gets deposited on the walls of the reactor. Therefore, the reaction chamber has to undergo periodic cleaning steps. In addition, the Cu foil is delicate to handle. At post-growth, a minor mishap can cause it to bend and, ultimately, compromise the structural quality of the graphene on it. Besides, the financial and environmental challenges using metal foils are also notable. At industrial scale, the waste would be considerable because the sacrificial catalytic metal sheets are used in the range of 25 to 50 µm in thickness [13, 14]. In view of this, alternative processes to grow graphene by CVD include the use of thermally-deposited Cu films on SiO_2/Si or sapphire substrates [15, 16]. This approach is promising for electronic and gas-sensing devices as these requires straightforward transfer and large-area of the active materials [17]. However, due the high-temperature instability at of the deposited Cu films (resulting from the inter-diffusion of Cu and SiO_2), the growth of uniform, continuous and large area graphene continues to be elusive. Recently, Howsare et al. proposed that a 50 nm Ni film could act as a barrier layer to minimize the inter-diffusion of Cu and SiO_2 [15]. This could be an important step towards producing tens of cm^2 graphene films required for scaling of gas sensing.

Highly, hazardous gases such as NO_2 and NH_3 are produced daily by various industries. This situation demands fast, reliable and low-cost gas sensing solutions. The gas-sensing properties of graphene were first investigated by Novoselov *et al.* [18]. They demonstrated that a graphene-based sensor (prepared using micromechanical cleavage of graphite) was able to detect of adsorbed individual molecules of NO_2 and NH_3. Interestingly, these authors relied on a Hall geometry gas sensing device. To this day, challenges persist in reaching a sensitivity of that level when using graphene produced by other synthesis techniques and/or chemiresistor type devices (i.e. the simplest working design). Accordingly, efforts have included the use of chemically exfoliated graphene by tailoring the degree of oxidation, by decorating with inorganic nanoparticles, or by functionalizing with diverse organic moieties, polymers, etc. [9, 11, 19-23]. These approaches are suffer from various drawbacks, for instance, it is difficult to reliably reproduce the oxidation degree for powdered graphene material [19, 24, 25]. Also, chemical exfoliation and/or decoration of graphene include cumbersome surface modification and coating steps. As concerns, CVD grown graphene was used by several research groups to achieve a NO_2 sensitivity in the range of few parts per million to parts per billion (ppm to ppb). However, these films and devices required special treatments such as metal oxide Schottky junctions [26], O_3 treatment [27], S doping [28], high operating/recovery temperatures (80 - 250°C) [28-30], etc. In summary, structural and chemical tailoring of the graphene surface provides additional sensitivity, it also brings in additional costs and fabrication complexity [9, 11, 19-23, 26-28].

Here, we report a simpler and less expensive workflow for FLG production and its device integration than other proposed methods for graphene-based gas sensing systems. We developed a wafer-scale growth of FLG on Cu/Ni films with high structural quality and purity. To demonstrate its direct application, the as-produced FLG was transferred onto a patterned array of Si nanopillars and used as active gas-sensing material. The unique FLG/Si nanopillar device showed excellent NO_2 detection results in ppm to ppb range.

2. Experimental details

Materials:

2.1 Growth

A 6” Si(001) wafer (test grade, University Wafer Inc.) was cleaned, with successive rinses of acetone and ethanol, in an ultrasonic bath. Following this, a 300 nm layer of silica (SiO_2) was deposited using inductively coupled plasma chemical vapor deposition (PlasmaLab 100, Oxford Instruments). Immediately after, the SiO_2/Si wafer was loaded into a themal evaporation chamber (PVD 75, Kurt J. Lesker) for Cu or Ni film deposition. The deposition was performed after pumping down the chamber to a base pressure below 10^{-6} mbar. Five wafers were prepared with different thickness of Cu and Ni films, as listed in **Table 1**. The processed wafers (hereafter, CNS = Cu/Ni/SiO_2/Si) were cut into sample-pieces of 1 to 50 cm^2. The samples were then placed in a thermal CVD system (BM Pro 4”, Aixtron GmbH) and annealed for 10 to 30 min (at 900°C and using an H_2/N_2 atmosphere with flows of 1000/250 sccm, respectively). To promote the growth of graphene, a mixture of H_2 (100 to 1000 sccm) and CH_4 (5 to 100 sccm) was used at 930 to 950°C. The reaction times were varied from 2 to 10 min. The chamber pressure was maintained at 10 mbar throughout the process. Finally, the samples were cooled down under a mixed flow of H_2 and N_2, at 1000 sccm each. For reference, a cut piece of an as-received 25 µm thick Cu foil (99.95% purity, Alfa Aesar) was placed in the reaction chamber, next to the CNS samples, during initial annealing/growth runs.

2.2 Characterization

Pictures of the graphene samples were taken with a standard digital optical camera. To measure the surface root mean square (RMS) roughness of the Cu/Ni films, atomic force microscopy, AFM (Dimension Icon, Bruker) was used in intermittent contact mode. The morphological analysis was performed using scanning electron microscopy, SEM (Nova Nano, Thermo Fisher Scientific). The microstructure and elemental analysis of the Cu/Ni films were examined using transmission electron microscopy, TEM (Titan, Thermo Fisher Scientific, operated at 300 kV) and energy dispersive X-ray spectroscopy, EDX. To prepare the cross-sectional TEM lamella, SEM with a focused ion beam (FIB) source was employed (dual-beam Helios 650, Thermo Fisher Scientific) and followed a standard *in-situ* lift-out method [31]. The grain orientation distribution was studied using electron backscatter diffraction, EBSD (Quanta 3D, Thermo Fisher Scientific). The structural analysis of the as-deposited samples was carried out with powder X-ray diffraction, XRD (D8 Advance DaVinci, Bruker, with a Cu Kα source, 1.5418 Å). To identify and characterize

the graphene films, Raman spectra were collected at 1 mW power (Alpha 300 RA, WITeC, 532 nm laser).

2.3 Graphene transfer

The as-grown FLG was transferred using a classical polymethyl methacrylate (PMMA)-assisted method [13]. Firstly, the graphene/CNS sample was spin coated with ~200 nm PMMA and, then, floated on a buffered oxy-etchant solution (6:1 volume ratio of 40% NH_4F in water to 49% HF in water). This overnight etching step was done to remove the SiO_2 layer, thereby detaching the Si substrate from the heterostructure composed by the stacked layers of graphene and catalyst. Following this, the CuNi alloy was dissolved (also overnight) by keeping it in a solution of H_2O (250 ml), HCl (2.5 ml) and H_2O_2 (2.5 ml). Afterwards, the remaining PMMA/graphene film was transferred onto different substrates, namely alumina, SiO_2/Si and, for the gas sensing experiments, patterned arrays of Si nanopillars (with native oxide layer on top). The nanopillars were fabricated on a highly-resistive Si wafer, as described elsewhere [32]. Finally, the PMMA was removed using a combination of UV-exposure, methyl isobutyl ketone (MIBK) and warm acetone [13].

2.4 Device fabrication and testing

First, the as-grown FLG was transferred onto a patterned array of Si nanopillars, as per the procedure explained above. Then, an alumina substrate (which included a screen-printed heating resistor) was glued, with a thermally conductive and electrically insulating epoxy resin, to the backside of the patterned SiO_2/Si die. This set-up was used to control the operating temperature of the device. The assembly was wire-bonded to a 2 × 3 cm^2 printed circuit board (PCB). Then, a silver epoxy paste (Heraeus) was employed to attach two platinum wire contacts on the graphene surface. The resulting planar electrode configuration enables monitoring of the electrical resistance of the nanopillar-supported graphene assembly. This process was selected to avoid contamination or damage to the graphene during the patterning of electrodes. Finally, the assembled and wire-bonded device was connected to a Teflon airtight chamber, linked to a mass-flow controller system (Bronkhorst, High-Tech B.V., Netherlands) and a multimeter (HP 34972A, Agilent), to record the changes in film resistance upon exposure to a gas flow. Calibrated gas cylinders of NO_2, NH_3 and synthetic dry air (purity: 99,995%) were used during the gas detection experiments. Well controlled NO_2 and NH_3 flows of 25 ppb to a hundred parts per million (ppm) were employed [33]. Due to limitations in our experimental setup, it was not possible to go below 25 ppb. The response

and recovery dynamics of sensors were studied (see **Figure SI1** and description) and it was found that reaching a steady state response to a stepwise change in gas concentration would take about 180 min. To speed up the gas sensing characterization process, the measurement strategy was implemented as follows. The sensor baseline resistance was stabilized in dry air for 1 hour to test different concentrations of a given gas. Then, a selected gas concentration (obtained via dilution and employing the mass-flow controller system) was delivered to the test chamber for 30 minutes. Meanwhile, the resistance changes were monitored at room temperature (RT = 25ºC, measured and monitored constant throughout the measurements). The response was recorded as $\Delta R/R_0$, where ΔR is the resistance variation experienced by the film during the 30 min exposure to a given gas concentration and R_0 is the baseline resistance in dry air. After this measurement, a 1 hour cleaning cycle in dry air was applied. This was done before performing measurements with a different gas concentration. The power source (E3648A, Agilent) was connected to the screen printed heater to raise the operating temperature of the sample. This allowed us to heat-up the sample to 100ºC while maintaining the overall chamber temperature at RT. Besides this, an evaporator and mixer (Bronkhorst, High-Tech B.V., Netherlands) were employed to adjust the humidity during some of the gas detection tests. The relative humidity (RH) level achieved inside the test chamber was verified employing a commercially available humidity sensor (E+E Electronics, Austria) placed at the vicinity of the device.

3. Results

3.1 Graphene growth optimization

Here, we expanded on Howsare *et al.* work [15], and evaluated the effect of the Cu and Ni films thickness in achieving wafer-scale growth of graphene by CVD. **Figure 1** shows representative SEM micrographs of the samples obtained via the following growth steps: 1) sample annealing at 900°C, for 10 min, 2) graphene growth at 940°C and using a H_2:CH_4 ratio of 1.5, for 10 min. To compare our graphene synthesis technique with the standard CVD graphene grown on Cu foil, a piece of a 25 µm thick Cu foil was placed beside the CNS samples. **Figure 1a** shows the presence of a significant number of spherical nanoparticles on the Cu foil surface after the growth step. This indicates that the Cu foil needs a pre-cleaning step, as explained elsewhere [13]. By contrast, there was no particle formation on the CNS samples (**Figures 1b to f**). For the N2S sample (**Figure 1b**),

the formation of Ni grains with few tens of nm was observed. On the sample surface, different image contrast was observed. Raman spectroscopy confirmed that the darkest area (marked with a red arrow) in **Figure 1b** corresponds to multi-layer graphene (not shown). The fainter area (top-left corner of **Figure 1b**) was identified as FLG whereas the lighter area did not show the presence of graphene. This agrees with previous reports confirming that it is rather difficult to control the number of graphene layers on a Ni substrate [34]. On the other hand, looking at the CNS, the surface texture is fairly uniform. For the C2N1S sample, no grain formation was noticed. However, the surface looks damaged (**Figure 1c**). For the other three samples, µm-sized grains were observed (**Figures 1d, e, f**) as well as holes which appeared in the thicker Cu films (500 nm) with a Ni barrier layer (100 or 200 nm) (**Figures 1e, f)**. Interestingly, for the C2N2S, these holes were rarely observed (**Figure 1d**). No full coverage of graphene was observed, except black patches were present in some areas. Using Raman spectroscopy, graphene was detected only in those areas of the C2N2S.

From above, the C2N2S-type samples were considered the most stable at the graphene growth conditions employed. Therefore, these samples were used to optimize large area with full sample coverage graphene growth. Different reaction parameters were explored, as detailed in **Figure SI2** and corresponding description. Briefly, the growth conditions were improved by introducing CH_4 (at 930°C) after the annealing step (at 900°C) for 30 min and ramping the temperature (to 950°C) for a graphene growth time of 10 min (**Figure 2a**). The results are presented in **Figures 2b to d**. SEM and Raman spectroscopy analyses were performed at different locations over a quarter of a 6" Si wafer (~50 cm^2), as shown in the inset of **Figure 2b**. The low magnification SEM image (**Figure 2b**) provides an overview of the sample revealing no surface defects or damage. The corresponding high-resolution image (**Figure 2c**), showed the presence of 1 - 3 µm grains on the surface. Optical microscopy (**Figure 2d**) carried out on an identical sample, showed areas with three different shades (dark, faint and light). Typical Raman spectra recorded at these areas are presented in **Figure 2e**. As expected, the two main characteristic peaks of graphene were observed: the 2D band, located at ~2700 cm^{-1}, and the G band, centered at ~1580 cm^{-1}. Thus, with a 2D to G peak intensity ratio of 1 and 0.6, the light and faint areas correspond to bi-layer and tri-layer graphene (BLG and TLG), respectively. The dark regions correspond to multi-layer graphene (MLG). The lack of a D peak confirms the growth of graphene with high structural quality. In fact, only two dark patches (with a few μm^2) are visible over a 252 μm^2 area (**Figure 2d**). This indicates

the dominance of FLG over the entire sample surface. The effect of the annealing step on the topography and surface microstructure of the CNS samples was studied using AFM and EBSD, respectively (refer to **Figures SI3, SI4 SI5** and corresponding descriptions). The majority of the *fcc*-Cu grains with large size (1- 3 μm) had the (111) planes parallel to the surface (**Figure SI5**), an orientation known to be favorable for SLG growth [35]. In these circumstances, we achieved uniform FLG on the C2N2S samples, i. e. without surface structural defects such as particle formation and/or agglomeration, holes, etc. (**Figure 2**). Henceforth, the growth conditions in **Figure 2a**, will be considered as the optimized conditions to grow high quality FLG.

3.3 Structural characterization of the optimal C2N2S samples

The XRD, presented in **Figure 3** shows diffraction peaks at 2θ = 44.1º, 51.6º and 75.2º, which match closely to the (111), (200) and (220) planes, respectively, of the $Cu_{2.7}$ $Ni_{1.8}$ $Si_{0.4}$ alloy (JCPDS data PDF 65-7517). However, and as discussed later, the localized EDX analyses on the cross-sectional TEM lamella (**Figures 4** and **SI6**), did not show the presence of Si in the Cu/Ni film region. Therefore, rather than the $Cu_{2.7}$ $Ni_{1.8}$ $Si_{0.4}$ phase, we refer to the formation of a Cu-rich CuNi alloy instead. The sharp (111) peak agrees well with the EBSD results (**Figure SI5**). Two other peaks, at 2θ = 33º and 69.5º, correspond to the SiO_2/Si substrate [36]. Thus, the Ni barrier layer prevents inter-diffusion of Cu and SiO_2 by the formation of a Cu rich Cu-Ni alloy.

To understand the microstructural evolution of the Cu and Ni films, cross-sectional TEM imaging (**Figure 4**) was performed on the as-deposited and graphene grown C2N2S samples. **Figure 4a** is a low magnification image of the as-deposited C2N2S, where the presence of a boundary between the Cu and Ni layers is clearly visible (also confirmed with EDX mapping in this region, not shown). The TEM analysis (**Figure 4b)** of the C2N2S sample after the graphene growth suggests that during the annealing and growth steps, the Ni and Cu film underwent mixing and formed a solid solution (refer to **Figures SI6f-k**). This is in agreement with the change in the sample color (top layer of the graphene/C2N2S sample) observed with naked-eye: from a Cu-like brown to a grey hue (see sample photo, inset of **Figure 2b**). From **Figure 4b**, the Cu-Ni film appears crystalline in the vicinity of the surface. Fast Fourier Transform (FFT) of the Cu-Ni portion (marked with a dotted red square) is shown in the inset of **Figure 4b**. From this, the measured interplanar distance (d) is found to be 0.21 nm. The (111) interplanar distance is close to that of a $Cu_{3.8}Ni$ alloy, $d_{(111)}$ = 0.208 nm [37]. This result agrees with the XRD and indicates the formation

of a Cu-rich Cu-Ni alloy (**Figure 3**).The slight difference in the exact CuNi alloy phase determination can be explained by the fact that the XRD detection occurs over a few microns of depth (averaged signal over μm^3) while TEM characterization is more localized (few nm^2).

The EDX mapping of the FLG/C2N2S (**Figure SI6g-k**) shows a homogeneous distribution of Cu and Ni over the 400 nm film thickness. It supports the formation of a Cu-Ni solid solution during the annealing and growth steps. The formation of voids in the Cu and Ni film was not observed in the cross-sectional TEM images, confirming the absence of holes in the catalyst film (**Figure 2**). This result is attributed to strengthening of the Cu film, provided by alloying. The EDX mapping suggests that diffusion of Cu and Ni in SiO_2 did not occur. This agrees with the results of Howsare et al., who claimed that a 5 - 50 nm Ni film reduces the inter-diffusion of Cu and SiO_2 [15]. We, therefore, confirm that the main cause of the Cu film instability on SiO_2/Si is overcome by the addition of a Ni film that acts as a barrier buffer. It should be noted that the inter-diffusion phenomenon explained here is growth specific and bears no direct effect on the gas-sensing influence of FLG, explained next.

3.4. Characterization of transferred FLG

For most applications, the graphene grown by CVD usually needs to be transferred from the catalytic metal sheet/film to a desired substrate. A digital picture of the transferred FLG (with PMMA layer and Cu grids trapped underneath) onto an alumina substrate is shown in **Figure 5a**. After the removal of PMMA, the Cu grids were detached from the FLG layer **(Figure 5b)**. Except for the area that was covered with the grids, the presence of a continuous FLG film is obvious. A piece of about 2 cm^2 was extracted from a second FLG sample and transferred to the array of Si nanopillars. The homogeneity of this layer was assessed using SEM, AFM and Raman spectroscopy. The SEM images, displayed in **Figures 5c** and **d**, indicate that the graphene is present over a large extension of the Si nanopillars array. In **Figures 5d and e**, it is possible to distinguish the edge of the FLG and the nanopillars underneath it, revealing that the transferred layer is thin and transparent to the electron beam. Considering that the substrate had a 3D morphology, the absence of cracks in the graphene is remarkable and attests its mechanical resilience. Raman spectra characteristic of BLG and TLG were obtained when analyzing this layer (**Figure 5f**). The negligible D peak confirms the presence of a clean and high structural quality

FLG film. Alongside, the substrate peaks - of Si (520 cm^{-1}) and SiO_2 (hump at ~950 cm^{-1}) - were also seen. Overall, it was possible to mount a cm^2 FLG film on a three-dimensional substrate without compromising its structural integrity.

3.4 Gas sensing studies

Afterwards, the FLG/Si nanopillar sensor was exposed to repeated response and recovery cycles of NO_2 at 250, 500, 750 and 1000 ppb. The values of the sensor baseline resistance under dry or humid conditions either at room temperature or when operated at 100ºC are summarized in **Table S1** (supporting information). Overall, the device response increased with increments in gas concentration (**Figure 6**). The augmented response correlates with an better charge transport by the film implying a measurable interaction with the gas. In fact, in the absence of moisture and at RT, it is known that NO_2 molecules can be physisorbed on graphene (with an energy of 67 meV) besides acting as electron acceptors [38]. The transfer of electronic charges will increase the concentration of holes in shifting its behavior to a mild p-type semiconductor, i.e. with its Dirac point below the Fermi level [39]. When the operating temperature was increased from RT to 100ºC, a slight improvement in the response ($\Delta R/R_0$) to NO_2 was obtained (**Figure 6b**). Likely, the adsorption/desorption interaction is more intense which leads to more pronounced charge transfer between the gas molecules and the FLG [40]. Our results match well with those of Xie et al., who reported that the best working temperature for monolayer graphene is near 100ºC [40]. According to these authors, when the operating temperature is raised to 200ºC (or more), the response decreases because the desorption process dominates over the adsorption one. The detection of NO_2 in the presence of moisture was also studied and the response to NO_2 was always higher than under dry conditions (**Figure 6b**). The well-structured lattice of the FLG could account for this. When moisture is adsorbed, charge transfer from graphene to the H_2O molecule is expected[38] [18]. Accordingly, the simultaneous presence of NO_2 and H_2O increases the conductivity of the film, via an additive effect, since both molecules behave as electron acceptors over a p-type material. Further to this, it is interesting to notice that the best response occurs at RT. Possibly, and at 100ºC, the additive effect is weaker because the water molecules are more mobile and less likely to adsorb onto the graphene (i.e. they are in a higher vibrational energy state, hence with lower surface residency time). Considering the good reproducibility and stability of the NO_2 response in the 250 to 1000 ppb range, additional measurements down to ultra-low concentrations were performed

(**Figure SI7**). The device could reliably detect this gas at 25 ppb, a remarkable figure for a pristine graphene layer. Taken together, and at the optimum working conditions (RT and 50% RH), the NO_2 sensitivity of the chemiresistive FLG-based device was 1.5×10^{-2} % per ppb.

To better understand the sensing mechanism, the detection of NH_3 was also evaluated. The typical resistance changes experienced by our FLG sensor, under repeated cycles of NH_3 exposure and varied conditions, are shown in **Figure 7**. Repeated baseline recovery cycles were performed before each set of measurements. At 100ºC and dry conditions, the response pattern is highly reproducible and stable over long periods of time (**Figure 7a**). When compared to NO_2, a relatively lower response was observed. This is explained by the NH_3 molecules acting as electron donors and having a lower physisorption energy on graphene (31 meV) [41] [38]. In the presence of moisture, the NH_3 response was lower. It is worth noting that H_2O molecules can act as electron-acceptor or electron-donors, depending on the experimental conditions and the nature of the sensing film [Ref]. Although a donor behavior cannot be completely discarded, Hall measurements reveal that water molecules act as electron-acceptors in graphene gas sensors at room or moderate temperature (cited already? DOI: 10.1038/nmat1967 and 10.1038/s41598-017-05333-w). This is logical: since the H_2O molecules as electron acceptors (while NH_3 acts as an electron donor). Hence, there is an opposite effect that will cancel out major changes to the FLG conductivity. On the whole, the ammonia-to-graphene charge transfers are more pronounced at 100ºC and in the absence of moisture (**Figure 7b**). In the 25 to 100 ppm range, and at these optimum working conditions, the NH_3 sensitivity is 5.3 x 10^{-2} % per ppm. This is roughly three orders of magnitude lower than the NO_2.

Taking into consideration the sensitivities obtained for NO_2 and NH_3, the limits of detection (LOD) and quantification (LOQ) were estimated. The LOD is the lowest concentration that can be surely registered; in other words, the minimum change in the signal that can be clearly distinguished from noise. As for the LOQ, it represents the lowest concentration that can be quantified. A factor of 3 and 10 was applied for the LOD and the LOQ, respectively, establishing a noise level of 150 mΩ and employing the slope obtained in the linear regression for the optimum working conditions for NO_2 and NH_3 [42]. For NO_2, an LOD of 5 ppb and a LOQ of 16.7 ppb were calculated. For NH_3, these values were higher, at 1 ppm and 3.4 ppm, respectively. In both cases, the estimated limits

are below the gas exposure thresholds advised by the World Health Organization [43], making our FLG-based sensor a promising alternative to more expensive and cumbersome devices.

3.5 Discussion

Commonly, the high temperature exposure of Cu films deposited on SiO_2/Si substrates leads to a damaged surface due to the inter-diffusion of Cu and SiO_2 [15]. Our results show that this phenomenon is suppressed using a 200 nm barrier layer of Ni which, upon the annealing and growth steps, bonds with Cu. Besides eliminating inter-diffusion, the presence of Ni also increases the solubility of C in the catalytic layer. For this reason, the production of FLG took place rather than the self-limited monolayer growth usually observed on Cu [12].

Pristine graphene is often reported to possess limited responsiveness to gas molecules [44], as summarized in **Tables 2** and **3**. For our FLG layers, X-ray photoelectron (XPS, not shown) and Raman spectroscopies revealed that there were no oxygenated chemical groups or a high density of other carbon lattice defects. Still, the NO_2 sensitivity reported here is higher than that claimed for CVD graphene [29, 45] or highly defective graphene materials such as graphene oxide [46] [47] or reduced graphene oxide [48, 49], even when functionalized with chemical moieties or nanoparticles [21, 27, 50]. In fact, it is well-known that the presence of defects and functional groups in carbon nanomaterials represent additional sites for adsorption of NO_2 molecules [51]. Generally, these lattice imperfections correlate with higher gas adsorption energies, in which case it will be more difficult to recover the sensor baseline [51]. While our FLG layer did not have oxygenated groups or defects, it was made of BLG, TLG and MLG domains (**Figure 5f**). In these circumstances, we propose that the surface steps derived from the presence of these domains contributed to the notable gas response observed. These steps would not alter considerably the Raman and XPS spectral signatures but would be preferred adsorption sites for the gas molecules [52-54]. At RT, the sensing mechanism is dominated by charge transfer through physisorption of NO_2 and NH_3, because, if there was chemisorption of NO_2, we would not observe significant baseline recovery.

Here, it should be steered that unlike previous reports (**Tables 2 and 3**), the gas-sensing studies were carried out using low gas flows (100 sccm) and long reaction times (30 min), close to the

practical conditions of environmental monitoring sensors. The response/recovery is slow, which could be further improved by decreasing the dead volume in the airtight chamber or device miniaturization [DOI: 10.1002/anie.201903089]. Therefore, considering the high sensitivity obtained for low concentration of pollutants (**Table 2**), the as-produced FLG shows a high potential to be further optimized towards a commercial NO_2 gas-sensor for continuous environmental monitoring doi:10.3390/app8071118].

Finally, one other factor at the origin of the excellent sensitivity and reproducibility of the NO_2 detection, is the unique device configuration used. When compared to flat substrates [55], an array of nanopillars bears the advantage of providing access to the backside surface of the graphene layer, thereby increasing the exposed surface area of sensing material. In this respect, the active available area is almost doubled. Suspending the graphene could also assist in obtaining an excellent baseline recovery, even at moderate temperatures. Such a configuration prevents trapping of gas molecules underneath the sensing layer and allows for a faster evacuation ahead of the next detection cycle.

4. Conclusions

The growth of wafer scale (~50 cm^2) FLG with high structural quality was successfully achieved using Cu films deposited on SiO_2/Si and an optimized Ni barrier layer. The formation of a Cu-rich Cu-Ni alloy, during the annealing and growth steps, is key to minimize the Cu and SiO_2 inter-diffusion and controllably obtain FLG. The applicability of the as-produced graphene was demonstrated for NO_2 and NH_3 gas sensing, after transferring it onto an array of Si nanopillars. A remarkable response was observed for both gases. At RT and in the presence of moisture, NO_2 could be detected over a wide concentration range, with a calculated LOD of 5 ppb. Under similar conditions, a relatively lower sensitivity was observed for NH_3 (LOD of 1 ppm) but this was explained by the type of gas interrogated.

The CVD growth of the FLG and its device integration, as described, represent a more viable work-flow than previous approaches for the fabrication of graphene-based gas-sensing systems. Besides minimizing the financial and environmental costs, this work-flow does not compromise

critical properties such as sensitivity (for electron acceptor gases, e.g. NO_2) and avoids cumbersome steps such as graphene surface functionalization and particle loading.

Acknowledgements

This work was funded by the Masdar Institute (contract EX2016-000026) and KAUST (BAS/1/1346-01-01). We are thankful to Dr. Sozaraj Rasappa (Tampere University, Finland) for the patterned Si nanopillar substrate. GD is thankful to Leslie George (Khalifa University, Abu Dhabi) for technical support. E.L. is supported by the Catalan Institution for research and Advanced Studies via the 2018 ICREA Academia Award, by MINECO and FEDER under grant no. TEC2015- 71663R and by AGAUR under grant no. 2017 SGR 418.

References

[1] K.S. Novoselov, V.I. Fal'ko, L. Colombo, P.R. Gellert, M.G. Schwab, K. Kim, A roadmap for graphene, Nature, 490(2012) 192-200.
[2] A.C. Ferrari, F. Bonaccorso, V. Fal'ko, K.S. Novoselov, S. Roche, P. Boggild, et al., Science and technology roadmap for graphene, related two-dimensional crystals, and hybrid systems, Nanoscale, 7(2015) 4598-810.
[3] W. Wei, X. Zhou, G. Deokar, H. Kim, M.M. Belhaj, E. Galopin, et al., Graphene FETs With Aluminum Bottom-Gate Electrodes and Its Natural Oxide as Dielectrics, Ieee T Electron Dev, 62(2015) 2769-73.
[4] F. Bonaccorso, Z. Sun, T. Hasan, A.C. Ferrari, Graphene photonics and optoelectronics, Nat Photonics, 4(2010) 611-22.
[5] X.H. Cao, Y.M. Shi, W.H. Shi, G. Lu, X. Huang, Q.Y. Yan, et al., Preparation of Novel 3D Graphene Networks for Supercapacitor Applications, Small, 7(2011) 3163-8.
[6] F. Lang, M.A. Gluba, S. Albrecht, J. Rappich, L. Korte, B. Rech, et al., Perovskite Solar Cells with Large-Area CVD-Graphene for Tandem Solar Cells, J Phys Chem Lett, 6(2015) 2745-50.
[7] Z.Y. Yin, J.X. Zhu, Q.Y. He, X.H. Cao, C.L. Tan, H.Y. Chen, et al., Graphene-Based Materials for Solar Cell Applications, Adv Energy Mater, 4(2014).
[8] X.D. Wang, D.L. Gao, M.J. Li, H.J. Li, C.P. Li, X.G. Wu, et al., CVD graphene as an electrochemical sensing platform for simultaneous detection of biomolecules, Scientific reports, 7(2017).
[9] S.X. Yang, C.B. Jiang, S.H. Wei, Gas sensing in 2D materials, Appl Phys Rev, 4(2017).
[10] F. Yavari, N. Koratkar, Graphene-Based Chemical Sensors, J Phys Chem Lett, 3(2012) 1746-53.
[11] W.J. Yuan, G.Q. Shi, Graphene-based gas sensors, J Mater Chem A, 1(2013) 10078-91.

[12] X. Li, W. Cai, J. An, S. Kim, J. Nah, D. Yang, et al., Large-area synthesis of high-quality and uniform graphene films on copper foils, Science, 324(2009) 1312-4.
[13] G. Deokar, J. Avila, I. Razado-Colambo, J.L. Codron, C. Boyaval, E. Galopin, et al., Towards high quality CVD graphene growth and transfer, Carbon, 89(2015) 82-92.
[14] D.R. Cooper, B. D'Anjou, N. Ghattamaneni, B. Harack, M. Hilke, A. Horth, et al., Experimental Review of Graphene, ISRN Condensed Matter Physics, 2012(2012) 56.
[15] C.A. Howsare, X.J. Weng, V. Bojan, D. Snyder, J.A. Robinson, Substrate considerations for graphene synthesis on thin copper films, Nanotechnology, 23(2012).
[16] K. Hayashi, S. Sato, N. Yokoyama, Anisotropic graphene growth accompanied by step bunching on a dynamic copper surface, Nanotechnology, 24(2013) 025603.
[17] M.P. Levendorf, C.S. Ruiz-Vargas, S. Garg, J. Park, Transfer-Free Batch Fabrication of Single Layer Graphene Transistors, Nano letters, 9(2009) 4479-83.
[18] F. Schedin, A.K. Geim, S.V. Morozov, E.W. Hill, P. Blake, M.I. Katsnelson, et al., Detection of individual gas molecules adsorbed on graphene, Nature materials, 6(2007) 652-5.
[19] J.D. Fowler, M.J. Allen, V.C. Tung, Y. Yang, R.B. Kaner, B.H. Weiller, Practical Chemical Sensors from Chemically Derived Graphene, Acs Nano, 3(2009) 301-6.
[20] T.T. Tung, N.V. Chien, N. Van Duy, N. Van Hieu, M.J. Nine, C.J. Coghlan, et al., Magnetic iron oxide nanoparticles decorated graphene for chemoresistive gas sensing: The particle size effects, J Colloid Interface Sci, 539(2019) 315-25.
[21] M. Zhao, F.L. Dong, L.Q. Yan, L.H. Xu, X.F. Zhang, P.P. Chen, et al., High efficiency room temperature detection of NO2 gas based on ultrathin metal/graphene devices, Rsc Advances, 6(2016) 84082-9.
[22] S.L. Zhang, N.T. Hang, Z.J. Zhang, H.Y. Yue, W. Yang, Preparation of g-C3N4/Graphene Composite for Detecting NO2 at Room Temperature, Nanomaterials-Basel, 7(2017).
[23] B. Zhang, G.N. Liu, M. Cheng, Y. Gao, L.J. Zhao, S. Li, et al., The preparation of reduced graphene oxide-encapsulated alpha-Fe2O3 hybrid and its outstanding NO2 gas sensing properties at room temperature, Sensor Actuat B-Chem, 261(2018) 252-63.
[24] T.T. Wang, J.Y. Hao, S.L. Zheng, Q. Sun, D. Zhang, Y. Wang, Highly sensitive and rapidly responding room-temperature NO2 gas sensors based on WO3 nanorods/sulfonated graphene nanocomposites, Nano Res, 11(2018) 791-803.
[25] A. Alazmi, S. Rasul, S.P. Patole, P.M.F.J. Costa, Comparative study of synthesis and reduction methods for graphene oxide, Polyhedron, 116(2016) 153-61.
[26] V.V. Quang, N.V. Dung, N.S. Trong, N.D. Hoa, N.V. Duy, N.V. Hieu, Outstanding gas-sensing performance of graphene/SnO2 nanowire Schottky junctions, Applied Physics Letters, 105(2014).
[27] M.G. Chung, D.H. Kim, H.M. Lee, T. Kim, J.H. Choi, D.K. Seo, et al., Highly sensitive NO2 gas sensor based on ozone treated graphene, Sensor Actuat B-Chem, 166(2012) 172-6.
[28] L.F. Guo, T. Li, Sub-ppb and ultra selective nitrogen dioxide sensor based on sulfur doped graphene, Sensor Actuat B-Chem, 255(2018) 2258-63.
[29] H. Choi, J.S. Choi, J.S. Kim, J.H. Choe, K.H. Chung, J.W. Shin, et al., Flexible and Transparent Gas Molecule Sensor Integrated with Sensing and Heating Graphene Layers, Small, 10(2014) 3685-91.
[30] Y.H. Kim, S.J. Kim, Y.J. Kim, Y.S. Shim, S.Y. Kim, B.H. Hong, et al., Self-Activated Transparent All-Graphene Gas Sensor with Endurance to Humidity and Mechanical Bending, ACS nano, 9(2015) 10453-60.

[31] N.S. Rajput, S.-G. Kim, J.B. Chou, J. Abed, J. Viegas, M. Jouiad, Electron beam induced rapid crystallization of water splitting nanostructures, MRS Advances, 1(2016) 825-30.
[32] S. Rasappa, D. Borah, R. Senthamaraikannan, C.C. Faulkner, M.T. Shaw, P. Gleeson, et al., Block copolymer lithography: Feature size control and extension by an over-etch technique, Thin Solid Films, 522(2012) 318-23.
[33] G. Deokar, P. Vancso, R. Arenal, F. Ravaux, J. Casanova-Chafer, E. Llobet, et al., MoS2-Carbon Nanotube Hybrid Material Growth and Gas Sensing, Adv Mater Interfaces, 4(2017).
[34] A. Dahal, M. Batzill, Graphene-nickel interfaces: a review, Nanoscale, 6(2014) 2548-62.
[35] J.D. Wood, S.W. Schmucker, A.S. Lyons, E. Pop, J.W. Lyding, Effects of Polycrystalline Cu Substrate on Graphene Growth by Chemical Vapor Deposition, Nano letters, 11(2011) 4547-54.
[36] P.S. Lee, D. Mangelinck, K.L. Pey, Z.X. Shen, J. Ding, T. Osipowicz, et al., Micro-Raman spectroscopy investigation of nickel silicides and nickel (platinum) silicides, Electrochem Solid St, 3(2000) 153-5.
[37] N. Rajasekaran, S. Mohan, Structure, microstructure and corrosion properties of brush-plated Cu-Ni alloy, J Appl Electrochem, 39(2009) 1911-6.
[38] O. Leenaerts, B. Partoens, F.M. Peeters, Adsorption of H(2)O, NH(3), CO, NO(2), and NO on graphene: A first-principles study, Physical Review B, 77(2008).
[39] W. Zhang, L. Wu, Z. Li, Y. Liu, Doped graphene: synthesis, properties and bioanalysis, Rsc Adv, 5(2015) 49521-33.
[40] H.F. Xie, K.K. Wang, Z.Q. Zhang, X.J. Zhao, F. Liu, H.C. Mu, Temperature and thickness dependence of the sensitivity of nitrogen dioxide graphene gas sensors modified by atomic layer deposited zinc oxide films, Rsc Advances, 5(2015) 28030-7.
[41] G. Lee, G. Yang, A. Cho, J.W. Han, J. Kim, Defect-engineered graphene chemical sensors with ultrahigh sensitivity, Physical Chemistry Chemical Physics, 18(2016) 14198-204.
[42] A. Shrivastava;, V.B. Gupta, Methods for the determination of limit of detection and limit of quantitation of the analytical methods, Chron Young Sci, 2(2011) 5.
[43] https://www.who.int/en/news-room/fact-sheets/detail/ambient-(outdoor)-air-quality-and-health.
[44] F.L. Meng, Z. Guo, X.J. Huang, Graphene-based hybrids for chemiresistive gas sensors, Trac-Trend Anal Chem, 68(2015) 37-47.
[45] C. Lee, J. Ahn, K.B. Lee, D. Kim, J. Kim, Graphene-based flexible NO2 chemical sensors, Thin Solid Films, 520(2012) 5459-62.
[46] C. Piloto, M. Notarianni, M. Shafiei, E. Taran, D. Galpaya, C. Yan, et al., Highly NO2 sensitive caesium doped graphene oxide conductometric sensors, Beilstein J Nanotech, 5(2014) 1073-81.
[47] L. Guo, Y.W. Hao, P.L. Li, J.F. Song, R.Z. Yang, X.Y. Fu, et al., Improved NO2 Gas Sensing Properties of Graphene Oxide Reduced by Two-beam-laser Interference, Scientific reports, 8(2018).
[48] H. Zhang, Q. Li, J.Y. Huang, Y. Du, S.C. Ruan, Reduced Graphene Oxide/Au Nanocomposite for NO2 Sensing at Low Operating Temperature, Sensors, 16(2016).
[49] P.G. Su, H.C. Shieh, Flexible NO2 sensors fabricated by layer-by-layer covalent anchoring and in situ reduction of graphene oxide, Sensor Actuat B-Chem, 190(2014) 865-72.
[50] L. Li, S.J. He, M.M. Liu, C.M. Zhang, W. Chen, Three-Dimensional Mesoporous Graphene Aerogel-Supported SnO2 Nanocrystals for High-Performance NO2 Gas Sensing at Low Temperature, Anal Chem, 87(2015) 1638-45.

[51] Y. You, J. Deng, X. Tan, N. Gorjizadeh, M. Yoshimura, S.C. Smith, et al., On the mechanism of gas adsorption for pristine, defective and functionalized graphene, Physical Chemistry Chemical Physics, 19(2017) 6051-6.
[52] A. Salehi-Khojin, D. Estrada, K.Y. Lin, M.H. Bae, F. Xiong, E. Pop, et al., Polycrystalline Graphene Ribbons as Chemiresistors, Adv Mater, 24(2012) 53-+.
[53] R.K. Paul, S. Badhulika, N.M. Saucedo, A. Mulchandani, Graphene Nanomesh As Highly Sensitive Chemiresistor Gas Sensor, Anal Chem, 84(2012) 8171-8.
[54] M.M. Pour, A. Lashkov, A. Radocea, X.M. Liu, T. Sun, A. Lipatov, et al., Laterally extended atomically precise graphene nanoribbons with improved electrical conductivity for efficient gas sensing, Nature communications, 8(2017).
[55] S.W. Lee, W. Lee, Y. Hong, G. Lee, D.S. Yoon, Recent advances in carbon material-based NO2 gas sensors, Sensor Actuat B-Chem, 255(2018) 1788-804.

Figures

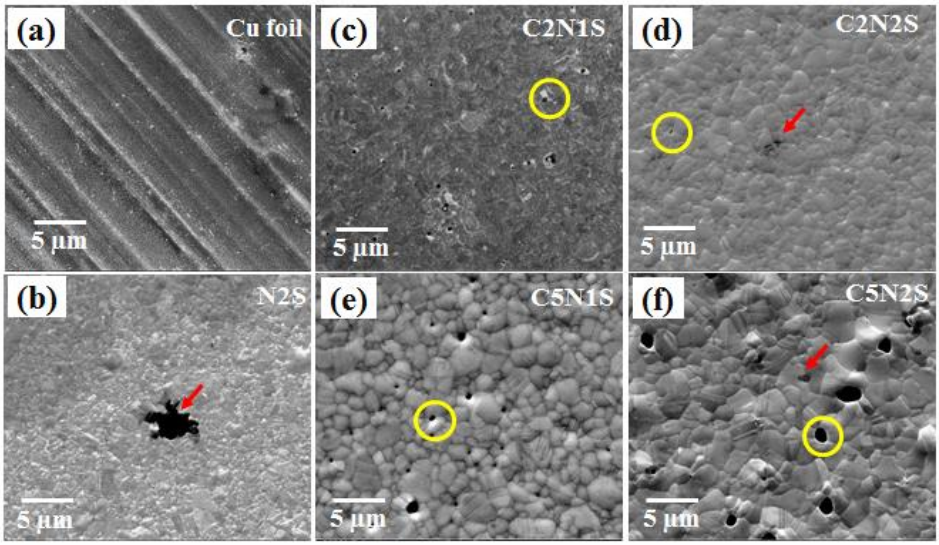

Figure 1. Graphene growth carried out on different samples (refer Table 1) with varied Ni and Cu thickness and 25 µm Cu foil with pre-annealing at 900℃ for 10 min and growth temperature 940℃, with H_2 to CH_4 flow ratio of 1.5 for 10 min. Typical dark patches of graphene are marked by red arrow. Typical holes in the CNS films are marked by yellow circle. Scale bar is same for all images as that of panel (a)

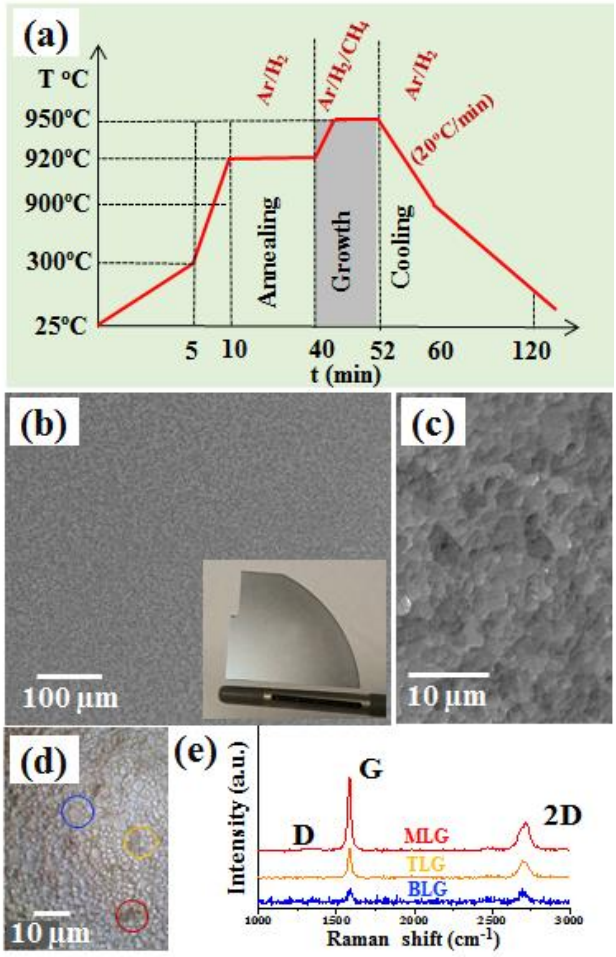

Figure 2. (a) Schematic of optimized growth recipe. SEM images of graphene grown on C2N2S at optimized growth conditions: (b) Low magnification image graphene growth with a photo of sample in the inset (quarter of 6" Si wafer), (c) High resolution image. (d) Optical microscopy image. (e) Raman spectra recorded at different positions on the image in panel (d) marked by red, orange and blue circles.

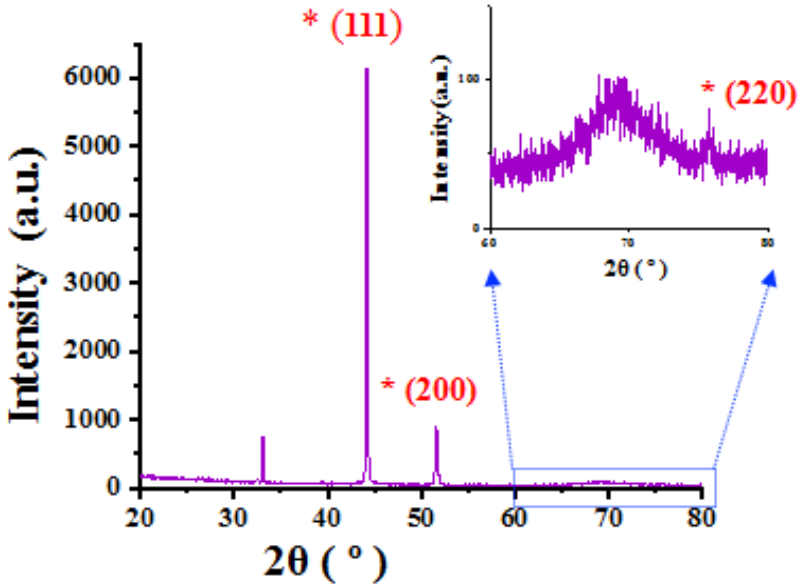

Figure 3. XRD spectra for C2N2S sample grown at optimized condition. Peaks marked with ' * ' corresponds to $Cu_{2.7}$ $Ni_{1.84}Si_{0.4}$ phase.

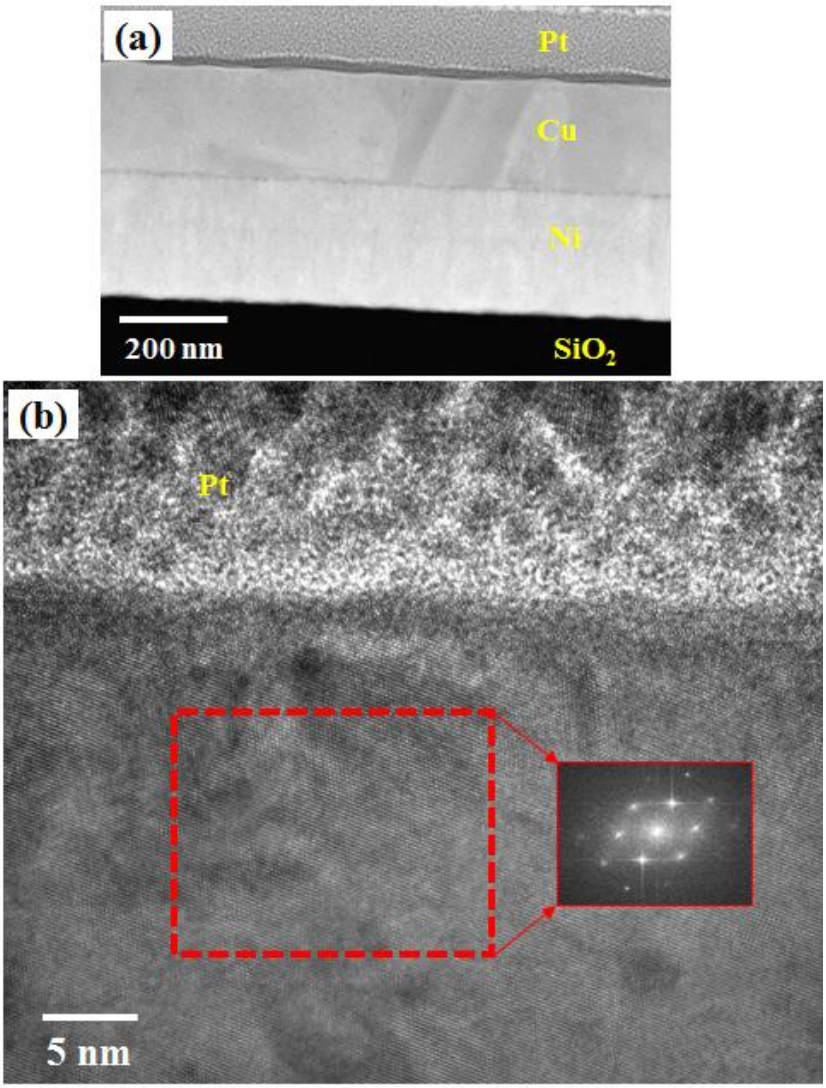

Figure 4. Cross-section TEM images for C2N2S sample: (a) Un-annealed film, (b) After FLG growth at optimized conditions with low resolution TEM image and FFT pattern for red dotted square in the inset.

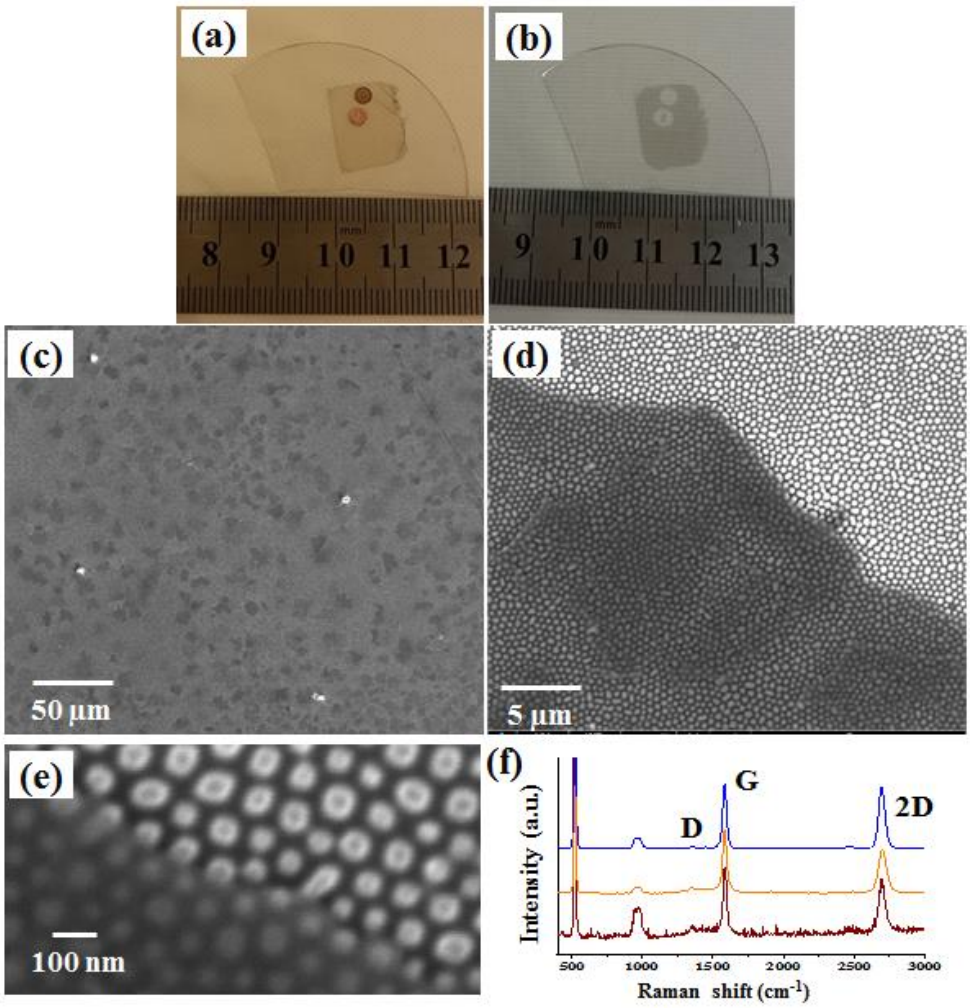

Figure 5. Digital photographs of FLG transferred on alumina: (a) PMMA/FLG with Cu grids underneath, (b) after PMMA and Cu grids removal. SEM images of FLG transferred on patterned SiO_2/Si nanopillar substrates: (c) Low resolution SEM image, (d) and (e) High resolution SEM images around the graphene edge. (f) Typical Raman spectra at different positions.

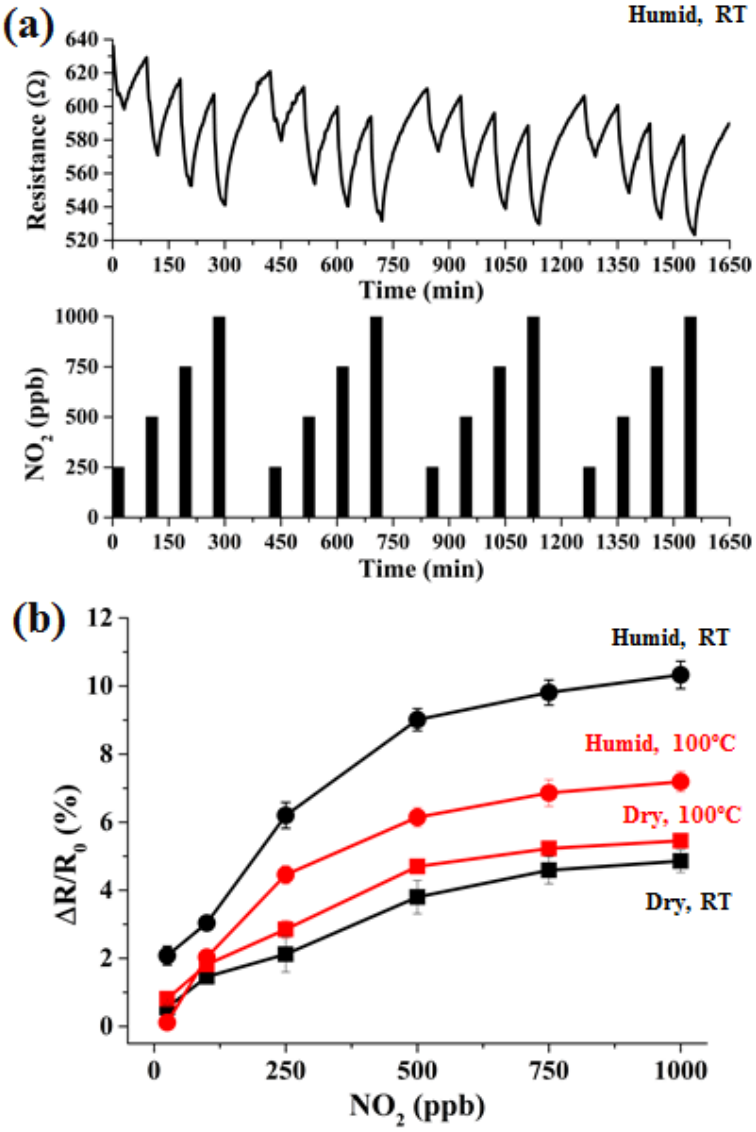

Figure 6. (a) Example of NO_2 detection at RT and under a RH of 50%. (b) Calibration curves obtained for NO_2 detection (black line: RT; red line: 100ºC; square symbol: dry conditions; circle symbol: 50% of RH).

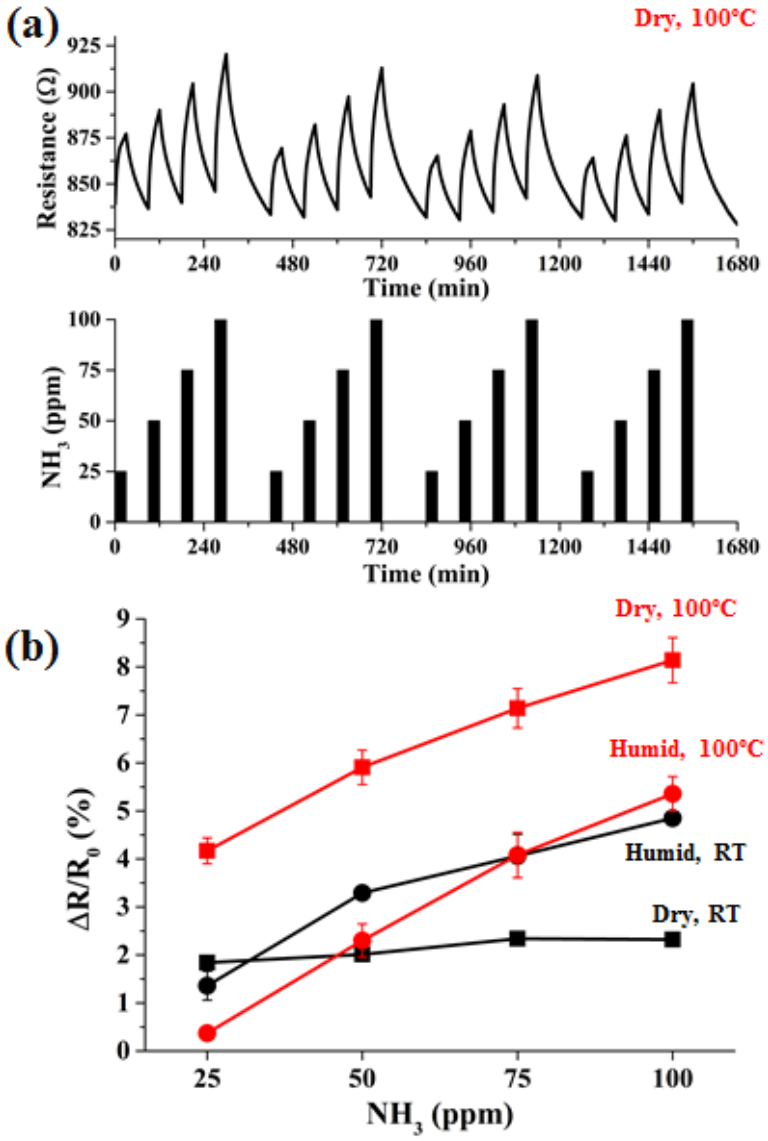

Figure 7. (a) Example of NH_3 detection at 100ºC in dry conditions. (b) Calibration curves obtained for NH_3 detection (black line: RT; red line: 100ºC; square symbol: dry conditions; circle symbol: 50% RH).

Tables

Table 1. Different samples were used for graphene growth. 300 nm SiO_2 on Si substrate was deposited with 100 or 200 nm Ni films. Afterwards, on the Ni films 200 nm or 500 nm Cu films were deposited. The short-forms for given Ni and Cu films decided as listed below.

Sample Short-form	Cu film	Ni film	Substrate
C2N1S	200	100	SiO_2 (300 nm) /Si
C5N1S	500	100	
C2N2S	200	200	
C5N2S	500	200	
N2S	0	200	

Table 2. Comparison of sensitivities to NO_2 expressed as 10^{-2} % /ppb in chemo-resistive sensors with dry air as a carrier gas. LCA: lowest concentration applied. R.H: study of relative humidity effect on gas sensing. NA: not available

Material	Synthesis technique	Additional preparation	T (°C)	Substrate	LCA (ppb)	LOD (ppb)	Sensitivity	RH	Reaction time (min)	Flow rate (sccm)	Reference (Year)
FLG	CVD	NA	RT	SiO_2 nano-pillars	25	5	1.5	Yes	30	100	This work
Graphene	CVD	S doping at 500˚C	RT	Micro-hotplateform	1000	NA	0.07	No	10	1000	[28] (2018)
Graphene	CVD	Electron beam lithography - plasma dry etching	RT	SiO_2	200	NA	0.25	No	3	500	[21] (2016)
Graphene	CVD	Photo-lithography and O_2 treatment	180	Polyimide	5000	7	-	Yes	NA	1000	[30] (2015)
Graphene	CVD	Graphene heater, Laser patterning	250	Polyethersulfone	500	NA	0.07	No	5	NA	[29] (2014)
Graphene	CVD	SnO_2 nanowire Schottky contact, 1V bias	120	SiO_2	10	0.024 ppt	0.09	No	<5	200	[26] (2014)
Graphene	CVD	Ozone treatment	RT	SiO_2	200000	1.3	0.0055	No	15	500	[27] (2012)
Graphene	CVD	Photo-lithography	RT	SiO_2	100000	NA	0.01	Yes	50	NA	[10] (2012)
Graphene	CVD	Lithography-RIE	RT	SiO_2	1000	15	0.43	No	15	200	[53] (2012)
Graphene	CVD	NA	-	PET	200000	NA	0.01	No	<5	NA	[45] (2012)
Graphene	Commercial graphite	Acid treatment enhanced liquid-phase exfoliation	RT	Alumina	5000	NA	0.22	No	NA	250	[22] (2017)
Graphene	Mechanical exfoliation	Hall geometry	120	SiO_2	0.2 ppb	0.06 ppt	1	Yes	60	NA	[18] (2007)
GO	Hummers method	Two-beam-laser interference	RT	Ceramic	4000	NA	0.15	No	<2	1000	[24] (2018)
GO	Commercial graphite	Graphene oxidation	RT	Alumina	3 ppm	90 ppb	0.51	No	4	200	[46] (2014)
rGO	Hummers method	rGo-Fe_2O_3 hybrid preparation	RT		5 ppm	NA	0.05	Yes	10	NA	[23] (2018)
rGO	Hummers method	Two-beam-laser interference	RT	Ceramic	4 ppm	NA	0.5	No	<1	NA	[47] (2018)
rGO	Commercial GO	Reduction of GO	RT	PET	1 ppm	NA	0.23	No	20	NA	[49] (2014)

Table 3. Comparison of sensitivities to NH_3 expressed as 10^{-2}%/ppm in chemo-resistive sensors with dry air as a carrier gas. LCA: lowest concentration applied. R.H: study of relative humidity effect on gas sensing. NA: not available.

Material	Synthesis technique	Additional preparation	T (˚C)	LCA (ppm)	LOD (ppm)	Sensitivity	RH	Reaction time (min)	Flow rate (sccm)	Reference (Year)
Graphene	CVD	NA	100	25	1	5.3	Yes	**30**	**100**	This work
Graphene	CVD	Photo-lithography and O_2 treatment	180	50	NA	5.4	Yes	**NA**	**1000**	[30] (2015)
Graphene	CVD	Electron beam lithography - plasma dry etching	RT	1	0.16	71	No	**15**	**200**	[53] (2012)
Graphene	CVD	Photo-lithography	RT	0.5	NA	83	Yes	**50**	**NA**	[10] (2012)
rGO	Commercial GO	Reduction of GO	RT	0.2	NA	5.5	No	**20**	**NA**	[49] (2014)